Advanced Robotics, Vol. 5, No. 2, pp. 183–205 (1991)

Impedance control of a direct-drive manipulator without using force sensors

SUSUMU TACHI,* TAISUKE SAKAKI,† HIROHIKO ARAI,** SHOICHIRO NISHIZAWA** and JOSE FELIPE PELAEZ-POLO‡

**RCAST, The University of Tokyo, 4-6-1 Komaba, Meguro-ku, Tokyo 153, Japan*
***Mechanical Engineering Laboratory, MITI, 1-2 Namiki, Tsukuba 305, Japan*
† Yaskawa Electric Mfg. Co. Ltd., 2346 Fujita, Yahatanishiku, Kitakyushu 806, Japan
‡ National University of Mexico

Received for *JRSJ* 5 July 1989; English version received 24 November 1989

Abstract—This research is concerned with impedance control of a manipulator which carries out stable contact tasks. The method controls the dynamic interaction between a robot and its environment by changing the apparent mechanical impedance of the manipulator. Conventional impedance control methods required force or torque sensors, which made the manipulator system very complex.

In this paper a new method is proposed for controlling the impedance of a manipulator without using force or torque sensors. The angular velocity and angular acceleration of the manipulator joints are estimated, and by using a computer model of the manipulator, the necessary torque for each joint is calculated and applied to the joint to attain the desired impedance. The feasibility of the method is verified by surface-following experiments and collision experiments using a two-degree-of-freedom direct-drive manipulator.

1. INTRODUCTION

The importance of using information not only of the position, but also of the force when controlling a manipulator to do a contact task has been discussed for a long time and many methods have been proposed and compared [1]. One typical method of force control is hybrid position/force control [2], but it retains many problems: selecting the position and the direction of controlling the position/force, sensing the boundary of an object, and switching the position/force mode in actual handling tasks.

Another typical method is impedance control. This is a control method based on the dynamic interaction between a robot and its environment; it is particularly effective in realizing stable force control in contact tasks. When a robot performs a contact task using this control, the relationship between the robot and its environment is regulated by impedance. Changes in the dynamic interaction between the robot and its environment are effected by changing the impedance. These appear as definitive changes in the apparent dynamics (inertia, viscosity, and stiffness) of the robot.

Impedance control is a generalized method [1] of stiffness control [3], compliance control [4], and damping control [5, 6]. Stiffness control and compliance control are similar to impedance control, but they deal only with static contact forces. Damping control, which is an expanded method of compliance

control, deals with a velocity effect but it does not imply a moment term. Otherwise, impedance control which changes a dynamic impedance is characterized by changing not only the stiffness and the viscosity, but also the apparent inertia of the end-effector.

This control method was systematized by Hogan [7], and was verified as being particularly effective when applied to contact tasks on highly rigid objects [8]. In addition, An and Hollerbach [9] have researched dynamic stability during force control. However, since previous impedance control methods use either force or torque sensors, the number of parts required in the manipulator is increased and the construction becomes very complex; then production cost is raised and the stiffness of the manipulator is reduced. Also, even if it has a force sensor, the external force of the parts of the tip of the manipulator can be measured, but the external force cannot be sensed on the other part of the tip of the manipulator.

Several methods for external force detection using no force sensors have been constructed by using only internal sensors. Inoue [10] and Kurono [11] proposed the position differential of a servo system for force detection. Uchiyama [12] applied his control method to a dynamic compensation method, and Arai and Tachi [13] developed an active power assistance method by using internal feedback. However, they did not make use of impedance.

This research proposes a new impedance control method using no force sensors. In this method, the angular velocity and angular acceleration of the manipulator joints are estimated, and by using a computer model of the manipulator, the torque necessary for each joint is calculated and applied to the joint in order to attain the desired impedance. An experimental 2-DOF (degree-of-freedom) DD (direct-drive) manipulator with vertical multiple articulation was constructed to test the effectiveness of this method. The feasibility of the method was demonstrated by surface-following experiments using the experimental hardware. In this method, the construction of manipulator is simplified by using no force sensors; the stiffness of the arm links is kept high; and the impedance can be controlled with external force on any parts of a manipulator.

2. IMPEDANCE CONTROL WITHOUT USING FORCE SENSORS

The manipulator's equation of motion is defined as follows:

$$I\ddot{\theta} + D_v\dot{\theta} + C(\theta, \dot{\theta}) = T_a + J^T F_e, \tag{1}$$

where I is the inertia matrix; D_v is the matrix of the viscous friction coefficients; and $C(\theta, \dot{\theta})$ is the gravity, Coulomb friction, and other non-linear terms.

The above coefficients can be easily identified for a DD manipulator. We will further define the notation as follows:

T_a : actuator output torque vector
F_e : vector of external force from the environment
θ : rotational angular vector of each axis
J : Jacobian matrix
J^T : transposed Jacobian matrix.

Next we will establish the target impedance $Z(j\omega)$ (multidirectional impedance

of the target position and posture X_0 of the end-effector) when contacting the environment. Here the impedance is defined using the analogy of voltage-force.

$$Z(j\omega) = B + j(M\omega - K/\omega). \tag{2}$$

The equation of motion for the system having a desired target impedance is expressed as follows:

$$F_e = M\ddot{X} + B\dot{X} + K(X - X_0), \tag{3}$$

where M is the virtual inertia matrix, B is the virtual viscous friction matrix, K is the virtual stiffness matrix, X is the position and posture vector in Cartesian space, $X_0 = X_0(t)$ is the virtual equilibrium point which shows the trajectory including target position and posture as a function of t.

Here, θ and X have the following relationship due to coordinate transformation:

$$X = L(\theta) \tag{4}$$

$$\dot{X} = J\dot{\theta} \tag{5}$$

$$\ddot{X} = J\ddot{\theta} + \dot{J}\dot{\theta}. \tag{6}$$

Substituting equations (4), (5), and (6) into equation (3), we obtain the following equation:

$$J^T F_e = J^T MJ\ddot{\theta} + J^T M\dot{J}\dot{\theta} + J^T BJ\dot{\theta} + J^T K(L(\theta) - X_0). \tag{7}$$

The output torque of actuator T_a needed to achieve the target impedance is calculated as follows:

$$T_a = (I - J^T MJ)\ddot{\theta} + (D_v - J^T M\dot{J} - J^T BJ)\dot{\theta} + J^T K(X_0 - L(\theta)) + C(\theta, \dot{\theta}). \tag{8}$$

If the manipulator's various coefficients have been identified, and if the motor's rotational angle, angular velocity, and angular acceleration can be measured from the sensors of the manipulator, equation (8) can be solved and the target impedance of equation (2) can be achieved.

Figure 1 shows a block diagram of the control system. In this diagram the term $C(\theta, \dot{\theta})$ is not shown.

If the trajectory X_0—position and posture—is a time function, the following method is used.

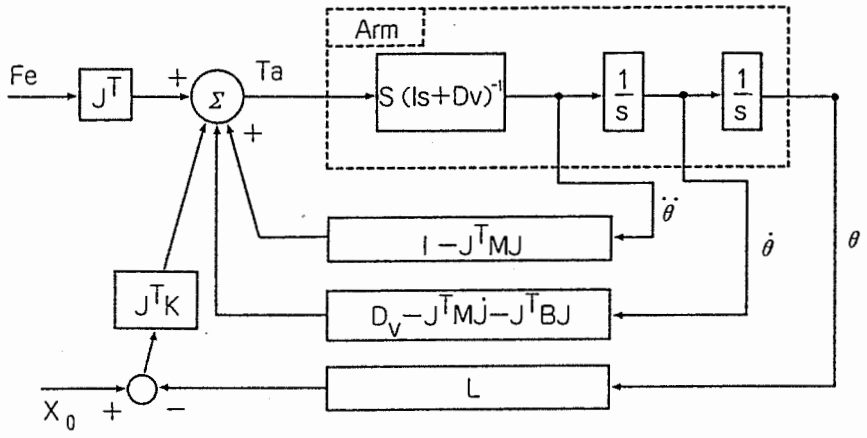

Figure 1. Block diagram of proposed impedance control.

When the commanded motion is $\ddot{X}_0, \dot{X}, X_0$, the dynamics of the system is changed by the feedback as follows:

$$F_e + F = M\ddot{X} + B\dot{X}, \tag{9}$$

where F_e is the external force; F is the force actuator torque transformed into a Cartesian coordinate system; and M, B are the target dynamics.

Then controlling the actuator torque, the following force is applied to the manipulator:

$$F = M\ddot{X}_0 + B\dot{X}_0 + K(X_0 - X). \tag{10}$$

With a given external force, the manipulator behaves with a target impedance at any time of motion as follows:

$$F_e = M(\ddot{X} - \ddot{X}_0) + B(\dot{X} - \dot{X}_0) + K(X - X_0). \tag{11}$$

Then the output actuator torque to realize the desired system is determined as follows:

$$\begin{aligned} T_a = {} & (I - J^T MJ)\ddot{\theta} + (D_v - J^T M\dot{J} - J^T BJ)\dot{\theta} \\ & + J^T M\ddot{X}_0 + J^T B\dot{X}_0 + J^T K(X_0 - L(\theta)) + C(\theta, \dot{\theta}). \end{aligned} \tag{12}$$

The block diagram is shown in Fig. 2. The term $C(\theta, \dot{\theta})$ is omitted in it.

Impedance control has so far been concerned with a contact task. Now a manipulator moving in free space is discussed.

The system dynamics is shown again as follows:

$$F_e + F = M\ddot{X} + B\dot{X}. \tag{13}$$

The trajectory is set as $\ddot{X}_0, \dot{X}_0, X_0$, and the control law is

$$F = M\ddot{X}_0 + B\dot{X}_0 + K(X_0 - X). \tag{14}$$

The whole system dynamics is shown as follows:

$$F_e = M(\ddot{X} - \ddot{X}_0) + B(\dot{X} - \dot{X}_0) + K(X - X_0). \tag{15}$$

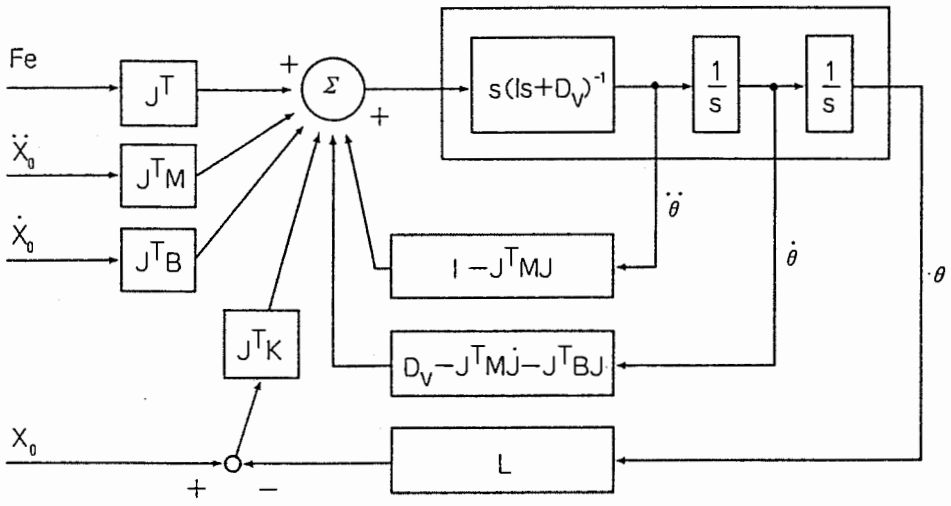

Figure 2. Block diagram of impedance control for desired general motion.

The external force is zero when the manipulator moves in free space:

$$F_e = 0. \tag{16}$$

Then the system moves as follows:

$$\ddot{e} + M^{-1}B\dot{e} + M^{-1}Ke = 0, \tag{17}$$

where

$$e = X - X_0. \tag{18}$$

In general, the error e is a six-dimensional vector:

$$e = \begin{bmatrix} e_1 \\ \vdots \\ e_6 \end{bmatrix}. \tag{19}$$

The error e converges stably and rapidly to zero under the following (critical damping) conditions:

$$(M^{-1}B)^2 = 4M^{-1}K \tag{20}$$

$$| sI + M^{-1}B/2 | = 0. \tag{21}$$

If the real parts of the root s of the characteristic equation are set to be negative with absolute values sufficiently large, and the target impedance is determined to satisfy the upper conditions, the error converges stably and rapidly to zero and stable trajectory control is realized. Then the control is the same as the conventional feedback/feedforward control [14, 15]. Also, the target impedance can be changed under these conditions.

3. MANIPULATOR STRUCTURE

3.1. Hardware

Figure 3 is a general view of the experimental manipulator, and Fig. 4 shows its structure. This manipulator is a 3-DOF vertically articulated manipulator.

The actuators are direct-drive motors which are suitable for force control and the estimation of a model of the manipulator [16, 17]. At each axis a DC torque motor (Inland Co.) is used. The specifications are listed in Table 1.

The entire linkage is made of duralumin. Table 2 lists the weight and dimensions of each link.

In experiment 4.2, the first axis was fixed and it was used as a 2-DOF manipulator.

3.2. Control system and program

Figure 5 is a schematic diagram of the control system. The signal from the rotary encoder of each axis is fed into a computer. After computing the rotational angle, angular velocity, and angular acceleration, the proper gains shown in equation (8)

are multiplied, and the necessary motor torque is estimated and then output to the servo amplifier. Current control takes place at the servo amplifier.

A 8000 p/r rotary encoder is used at each axis. To control the manipulator according to equation (8), an accurate value must be measured or estimated for the angular velocity and acceleration. However, when trying to find these through the differential in pulse number, the accuracy becomes very poor owing to the small effective number at low angular velocity. In this control system, the pulse interval is measured at 1 MHz on a standard clock, and the reciprocal number is taken as the angular velocity [18].

The angular acceleration is estimated by using a derivative with a four-point differential algorithm from the angular velocity and through a low-pass filter.

The programming language C is used, and the control period is 2.0 ms.

3.3. Derivation of the equation of motion and identification of control parameters

It is not easy to construct a model of a general manipulator with gears because of its friction. Therefore very complex methods are used to estimate the compensatory

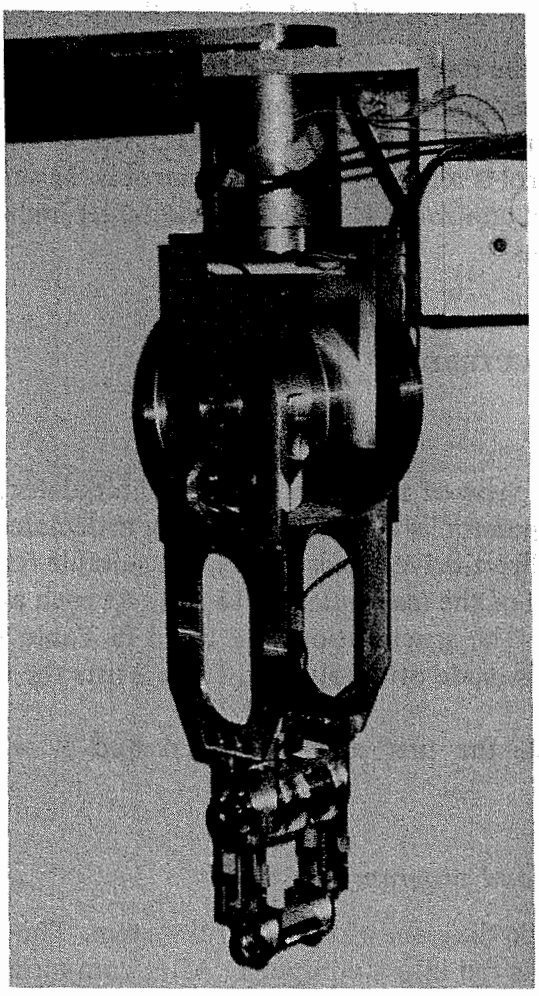

Figure 3. DD manipulator.

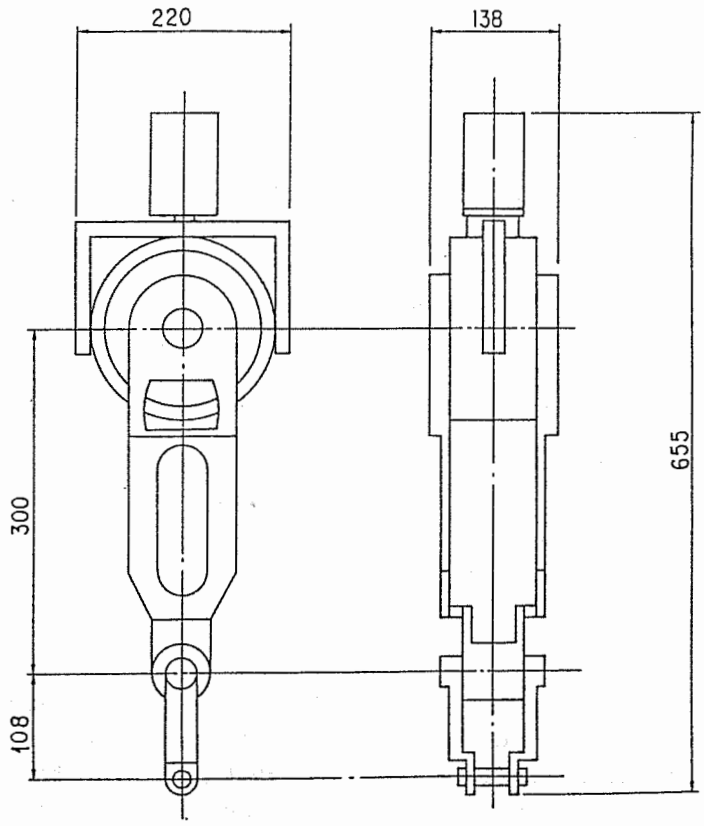

Figure 4. Configuration of the manipulator.

Table 1.
Specifications of DD motors

Joint	Peak torque (kg cm)	Speed (load = 0) (rpm)	Weight (kg)
1 (QT-2404A)	41.5	580	1.09
2 (QT-6202)	15.2	210	2.81
3 (QT-1406)	11.3	2989	0.34

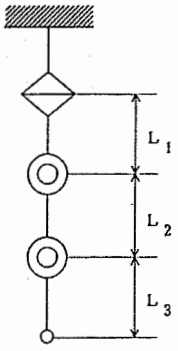

Table 2.
Specification of the links of the manipulator

	Length (m)	Weight (kg)
Link L_1	0.135	4.58
Link L_2	0.32	4.321
Link L_3	0.125	0.473

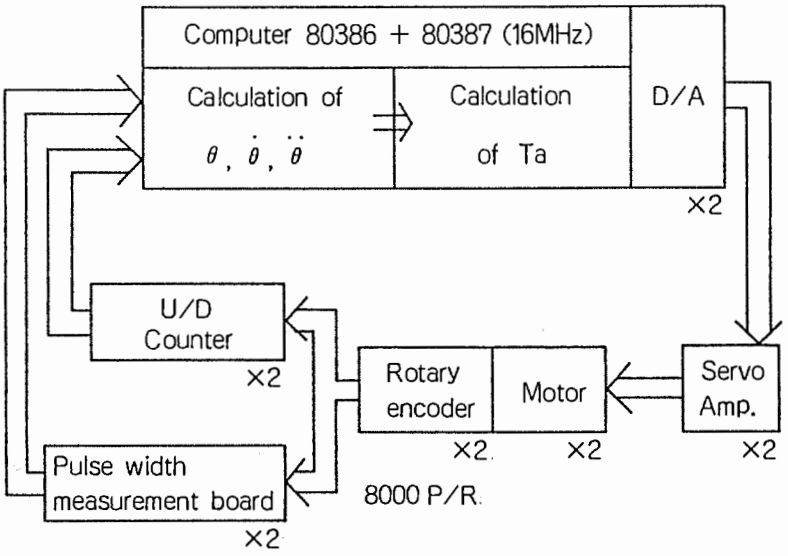

Figure 5. Control system of the manipulator.

value of its friction and interaction term. Onishi *et al.* [19] used an observer to compensate for the external force. In this paper, making use of the DD manipulator's torque, a simple method of modelling is available as follows.

The Lagrange method is used to derive the equation of motion for the manipulator (see Appendix 1).

A DD manipulator which has no friction or backlash is a system where ideally stiff bodies are linked freely at each joint. Therefore, if the equation of motion is expressed as in equation (A8), in order to identify its parameters, each axis is taken as the pivot of a pendulum and damped oscillation is performed separately on each link. From the experiment, the moment of inertia I, the viscous friction coefficient D_v, and the Coulomb friction C_r are derived.

The equation of motion for a rigid pendulum is expressed in the following equation:

$$I\ddot{\theta} + D_v\dot{\theta} + C_r = T_a - Mg \sin \theta. \tag{22}$$

Natural damping of the pendulum ($T_a = 0$) without driving the motors is often used when estimating the parameters by linear approximation of equation (22) on the assumption that θ is a minute angle and $\sin \theta = 0$. However, it is actually rather difficult to perform oscillation with a minute angle of θ; and actual viscous friction must be measured while driving the motors. Therefore, this natural damping of the pendulum is not used, and the parameters are identified by the following method.

First, the virtual spring coefficient K is introduced; the motor torque is applied as follows:

$$T_a = Mg \sin \theta - K\theta. \tag{23}$$

With this method, equation (22) is linearized by equation (23), and each parameter can be calculated accurately.

$$I\ddot{\theta} + D_v\dot{\theta} + C_r = -K\theta. \tag{24}$$

Table 3.
Estimated parameters of the equation of motion

Joint	Inertia (kg m ^{2})	Viscous damping coefficient (N m/(rad/s))	Coulomb friction (N m)
1	0.72	0.0022	0.1057
2	0.1871	0.057	0.4998
3	0.0351	0.001	0.0031

The parameter identification method is given in Appendix 2. Table 3 lists the parameters identified for each axis.

To operate this manipulator within the vertical plane, gravitational compensation was also performed.

4. CONTROL EXPERIMENTS

4.1. Control experiment with a one-degree-of-freedom manipulator

Using the parameters for the equation of motion of each axis found in Section 3.3, impedance control was performed on each link. The purpose of this experiment was to confirm that control was achieved according to the target impedance for each link, and to verify that the parameters for each axis were correctly identified.

The equation of motion of the system is

$$I\ddot{\theta} + D_v\dot{\theta} + C(\theta, \dot{\theta}) = T_a + J^T F_e, \tag{25}$$

and the desired target impedance is

$$Z(j\omega) = B + j(M\omega - K/\omega). \tag{26}$$

The desired equation of motion of a system with external force F_e and virtual equilibrium angle θ_0 is

$$J^T F_e = M\ddot{\theta} + B\dot{\theta} + K(\theta - \theta_0). \tag{27}$$

The output torque T_a for the actuator to attain the target impedance is

$$T_a = (I - M)\ddot{\theta} + (D_v - B)\dot{\theta} + K(\theta_0 - \theta) + C(\theta, \dot{\theta}). \tag{28}$$

Note that the coefficients given in (25)–(28) are scalar values.

There are two methods for assigning the desired target impedance (see Appendix 3). Here, however, the apparent interia ratio ϕ for the actual inertia, natural frequency f_r, and damping ratio ζ is set. The experimental values are those when step input is applied and the theoretical values are compared.

In this experiment control was performed using only link 2 as a 1-DOF manipulator with link 3 removed and axis 1 fixed. To assign the target impedance, the following parameters were set:

$\phi = 70\%$, $f_r = 2.0$ Hz, $\zeta = 0.1$, control period = 3 ms;
$\phi = 50\%$, $f_r = 2.0$ Hz, $\zeta = 0.1$, control period = 3 ms.

Figure 6 shows the results of the experiment. The solid line indicates the theoretical value, and the dotted line the experimental value. The double-dashed line shows the natural oscillation ($f_r = 0.781$ Hz, $\zeta = 0.028$) without control.

Even with 50% compensation for the inertia and a sampling period sufficiently short (3 ms), a response virtually identical to the desired impedance was achieved. This result confirmed the fact that proper identification of the parameters for axis 2 had been obtained.

The same results were also obtained when links 1 and 3 were controlled.

4.2. Control experiment with a two degree-of-freedom manipulator

Impedance control was next performed with a 2-DOF manipulator. The method for calculating the required torque for impedance control is given in Appendix 4. The following five control experiments were carried out:

(1) The compliance of the target impedance for the horizontal and vertical orientations was assigned, and the manipulator was made stationary at a virtual equilibrium point.

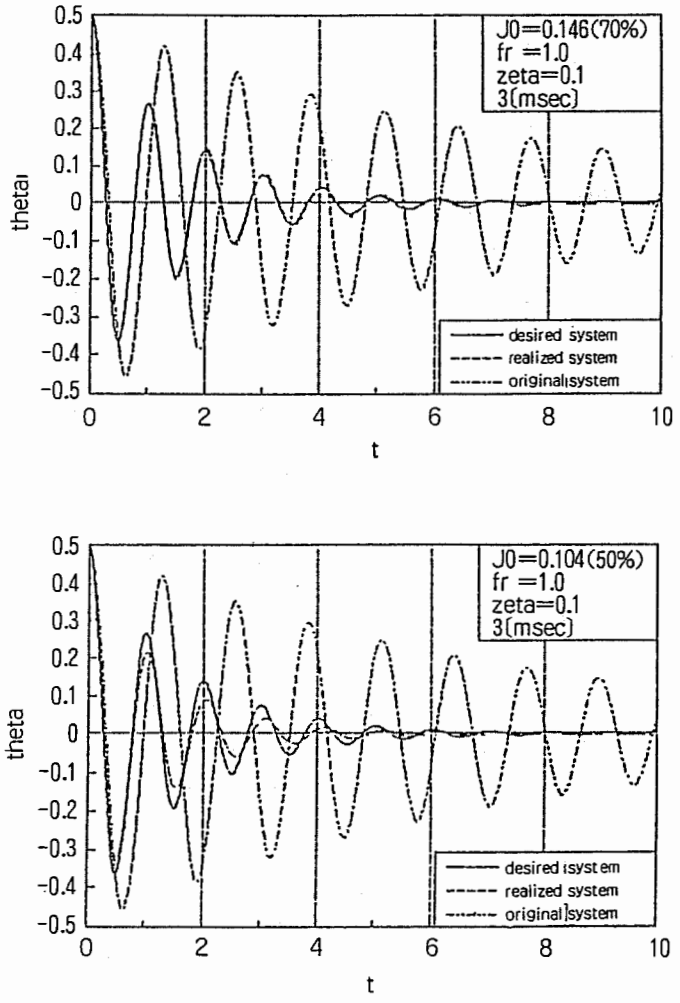

Figure 6. Experimental results of the impedance control for link 2.

The reaction force to the manipulator along the horizontal and vertical orientations is shown in Fig. 7. The graph shows the position deviations and reaction forces for the horizontal and vertical orientations, respectively.

The coefficient for each orientation was set as follows:

$K_y = 35.0$ N/m : spring coefficient for the horizontal orientation
$K_z = 35.0$ N/m : spring coefficient for the vertical orientation

As can be seen from the figure, the reaction force created is proportional to the positional deviation from the virtual equilibrium point. In this case, the impedance control can be regarded as compliance control.

(2) The target impedances for the horizontal and vertical orientation were set, and damped oscillation was performed at a given virtual equilibrium point.

The assigned impedance parameters for each orientation were

(i) $f_{r,y} = 1.0$ Hz, $\zeta_y = 0.1$;
$f_{r,z} = 1.0$ Hz, $\zeta_z = 0.1$;
(ii) $f_{r,y} = 1.0$ Hz, $\zeta_y = 0.1$;
$f_{r,z} = 2.0$ Hz, $\zeta_z = 0.1$;

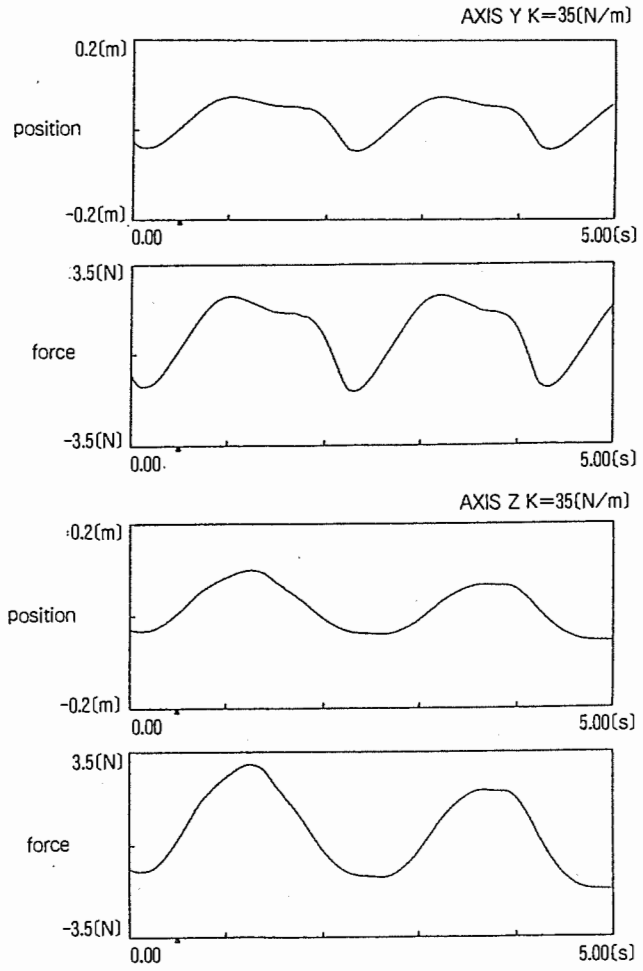

Figure 7. Experimental results of compliance control for horizontal and vertical orientations.

Note that the $\phi_y = 20\%$, $\phi_z = 5\%$ (total weight 4.727 kg), and the vertical equilibrium point is set at the position (0.125 m, -0.42 m).

The pendulum oscillations along the horizontal and vertical orientations are shown in Fig. 8. The solid line indicates the experimental values; the dotted line the theoretical values. From this result it can be seen that damped oscillation took place almost exactly according to the impedance assigned for each orientation.

The manipulator may oscillate when the assigned target impedance is beyond the limits of real actuator torque. Accordingly, it is necessary to determine whether or not the actuator can actually achieve the target impedance before actual control is performed (Appendix 5).

(3) The target impedances were set for each horizontal and vertical orientation, and the manipulator was moved along a horizontal surface while maintaining contact on the surface.

The assigned target impedances for each orientation were as follows:

$$\begin{aligned} \text{Natural frequency}: f_{r_y} &= 1.0 \text{ Hz}; \\ f_{r_z} &= 1.0 \text{ Hz}. \\ \text{Damping ratio}: \zeta_y &= 0.5; \\ \zeta_z &= 0.5. \\ \text{Ratio of the virtual mass of inertia}: \phi_y &= 10\%; \\ \phi_z &= 5\%. \end{aligned}$$

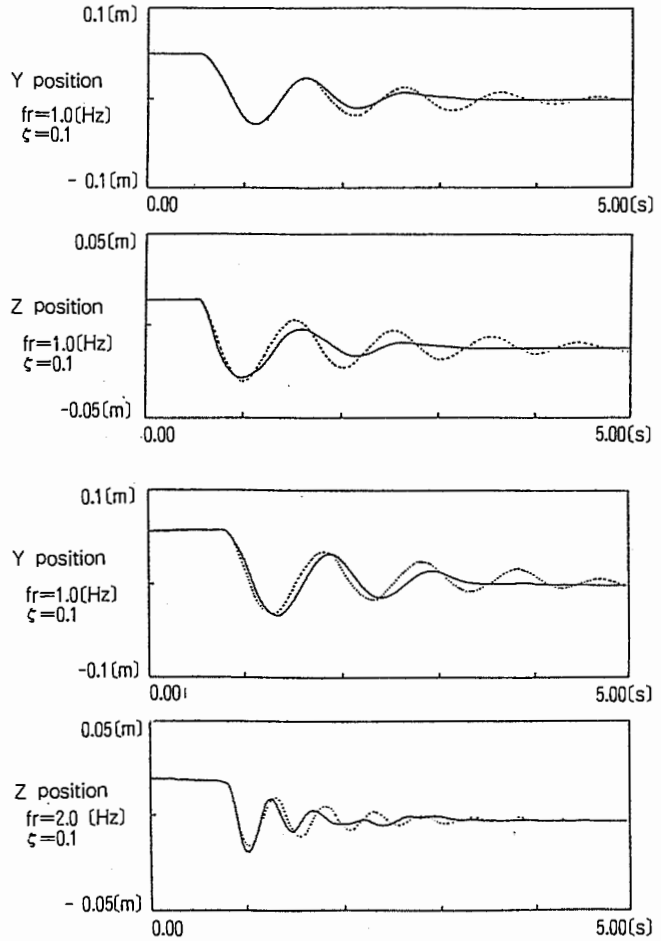

Figure 8. Experimental results of impedance control for horizontal and vertical orientations.

The working forces for the horizontal and vertical orientations as a function of time are shown in Fig. 9. The virtual equilibrium point is set just below the surface, and it is moved along the surface while maintaining a fixed distance from the surface. The manipulator exerts a fixed amount of vertical force on the surface and it follows the surface as it tries to follow the virtual equilibrium point.

(4) The manipulator avoids obstacles during the contact task. The same target impedances as those used in (3) were set, and the same operation was performed. The same straight line was set as a virtual trajectory. When a semicircular obstacle was placed on the surface, the manipulator followed the surface without changing the virtual trajectory. A force proportional to the positional variation from the virtual equilibrium point was applied to the obstacle, and it continued with its operation. The force applied to each orientation during the surface-following is shown in Fig. 10.

These graphs reveal that the value of the vertical orientation force along the time axis does not have a semicircular shape. This is because when the manipulator moves over a curved surface, a constant force is required along the tangent of the surface. Accordingly, when passing over the first half of the obstacle, the manipulator waits until the position differential from the virtual equilibrium point

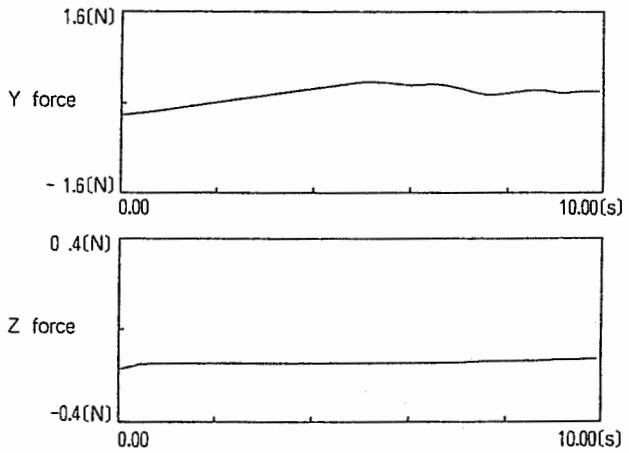

Figure 9. Experimental results of the working forces of impedance control on a flat surface.

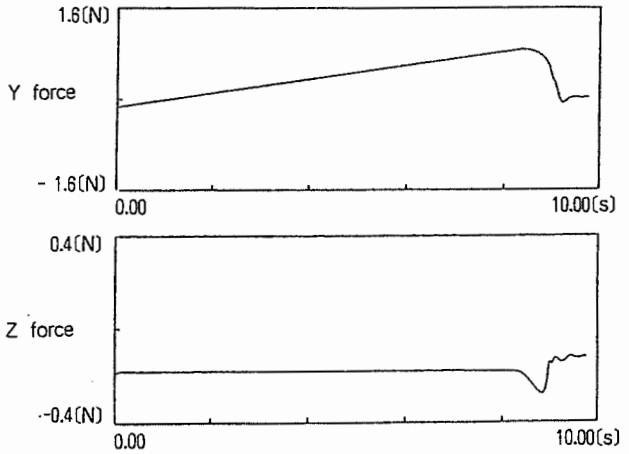

Figure 10. Experimental results of the working forces of impedance control on a semicircular obstacle.

has attained a sufficient amount of force along the tangent. When passing over the second half of the obstacle, the reverse of this occurs. If the mapping between the data with time and the contact surface is determined as follows, the actual contact surface can be reproduced.

The virtual equilibrium point is moved with velocity $V_y(t)$ applied to the horizontal orientation (axis Y). The velocity $V_z(t)$ is applied to the vertical orientation (axis Z), and the manipulator is moved at the composite speed. The relationship of the position differential between the virtual equilibrium point and the position of the end-effector, and the force to the environment (F_y, F_z) is expressed as follows:

$$F_y(t) = K_y \delta_y(t) \tag{29a}$$

$$F_z(t) = K_z \delta_z(t) \tag{29b}$$

where $F_y(t), F_z(t)$ are the forces for the Y, Z orientations; K_y, K_z are the spring coefficients for the Y, Z orientations; and $\delta_y(t), \delta_z(t)$ are the positional differential between the end-effector and the virtual equilibrium point for the Y, Z orientations.

The end-effector position is expressed as

$$y(t) = \int_0^t V_y(t)\,\mathrm{d}t - F_y(t)/K_y \tag{30a}$$

$$z(t) = \int_0^t V_z(t)\,\mathrm{d}t - F_z(t)/K_z. \tag{30b}$$

In the previous experiment, since $V_y(t) = V$, $V_z(t) = 0$,

$$y(t) = Vt - F_y(t)/K_y \tag{31a}$$

$$z(t) = -F_z(t)/K_z. \tag{31b}$$

Using the relationship in equation (31), the shape of the actual environment based on the experimental results was estimated. Figure 11 shows the result and the actual shape of the surface. It is shown that this method permits an accurate estimation of the shape of the environment.

It has been demonstrated that the manipulator can perform stable contact tasks while maintaining a desired target impedance.

(5) Transient response in a contact task was observed.

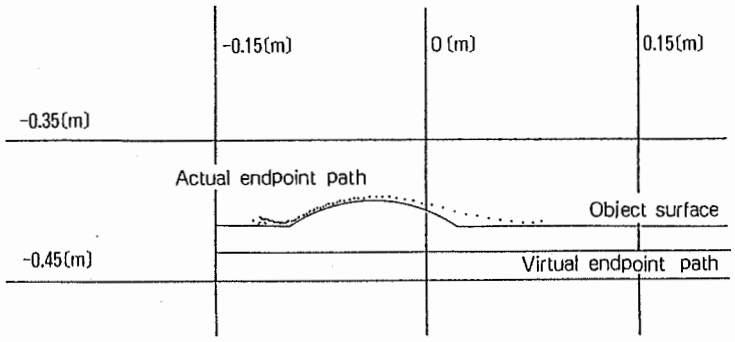

Figure 11. Surface following path of impedance control on an object.

While a static contact task is controlled in compliance control, dynamic interaction is controlled by changing the apparent inertia m in impedance control. Therefore, in impedance control, the impact of an object is reduced by changing the momentum mv with the same velocity v. For example, if the apparent inertia m is set small as a low impedance, the danger of destroying a manipulator or an object is reduced when the manipulator collides with the unexpected object at a high velocity. This method is possible because the trajectory-controlled manipulator moves in free space with low impedance.

Now the effect of the impact with a manipulator of reduced apparent inertia is verified in the next experiment.

The end-effector collided with a pendulum as an object with momentum mv, with apparent inertia m and constant velocity v (see Fig. 12). Then the motion of the pendulum was observed to estimate the practical inertia of the manipulator. But to prevent the destruction of the manipulator and to guarantee the regulation of the impedance, tennis balls were put on the pendulum.

The case where the apparent inertia was reduced with the acceleration signal—low impedance—was compared with the case where the inertia was not changed because the acceleration signal was not used. The pendulum oscillated in response to the momentum produced by the manipulator. The experimental result in Fig. 13 shows the dynamic effect of a reduced impedance, that the impact of a low impedance is smaller than that of a high one.

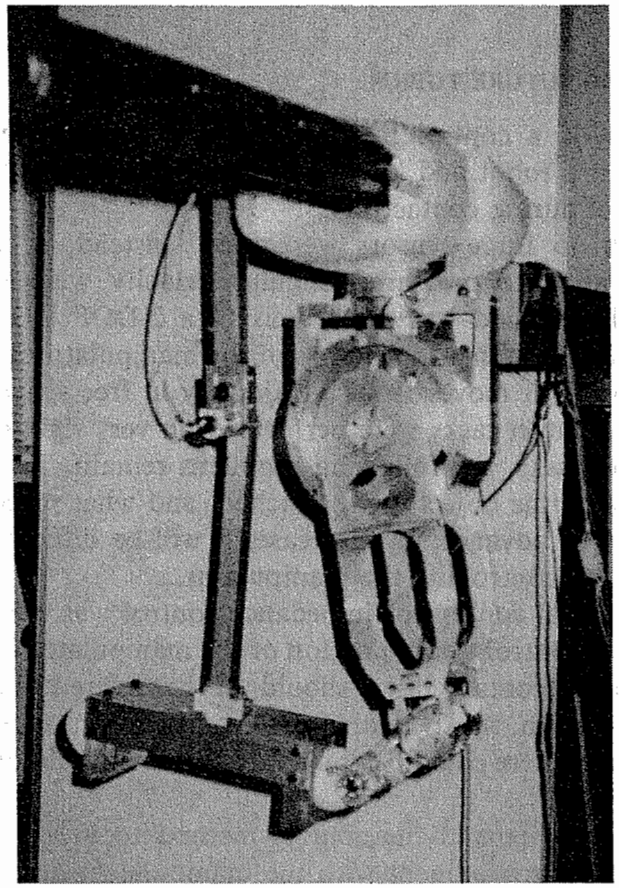

Figure 12. Experimental system for measuring transient response of collision.

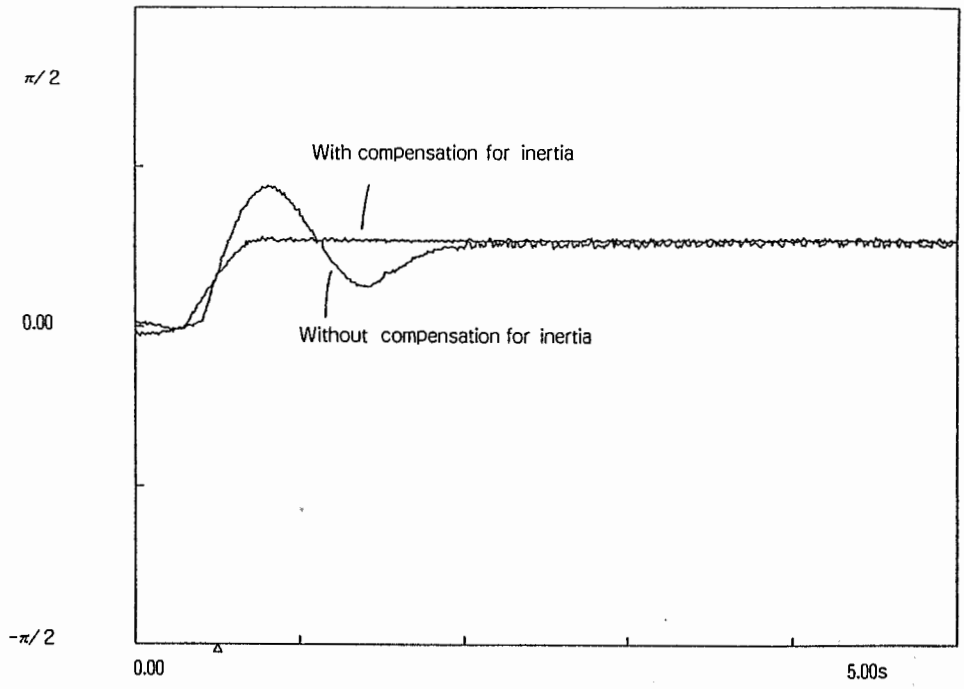

Figure 13. Experimental results of the dynamic effect of a reduced impedance.

5. CONCLUSION AND FUTURE TOPICS

Impedance control is a control method whose central concept is the dynamic interaction between a robot and its environment. In particular, it makes possible stable force control during contact tasks.

In this research no force sensors were used. Instead, a computer model of the manipulator and the measured angular velocity were exploited, and the effectiveness of the method was verified using a 2-DOF DD manipulator. This method has the advantage that the motion of the manipulator is controlled with the same impedance when it moves from a trajectory in free space to a contact task.

However, these contact tasks were performed on very rigid objects. When used for general contact tasks, the following problems remain. The dynamics (inertia, viscosity, stiffness) of the object being touched, and what place it will occupy are not usually known in advance. In that case, it will be difficult to perform stable contact tasks just by controlling the manipulator.

However, the central concept of impedance control was not just to control the manipulator, but to control a combination of the manipulator and its environment. In this way, general contact tasks should be considered. For example, if the environment is unknown, the dynamics of the environment must first be identified. The method proposed here could be applied to this 'manipulator plus environment' control.

The next step is to expand the control method to a 3-DOF manipulator, to identify an unknown environment with the manipulator, and to control both the manipulator and the environment impedance.

REFERENCES

1. D. E. Whitney, "Historical perspective and state of the art in robot force control," *Proc. IEEE Int. Conf. Robotics Automation*, pp. 262–268, 1985.
2. M. H. Raibert and J. J. Craig, "Hybrid position/force control of manipulators," *ASME J. Dyn. Syst. Meas. Control*, vol. 102, pp. 126–133, 1981.
3. J. K. Salisbury, "Active stiffness control of a manipulator in Cartesian coordinates," *Proc. IEEE Int. Conf. Decision Control*, vol. 1, pp. 95–100, 1980.
4. H. Hirabayas *et al.*, "Virtual compliance control of a multi-degree of freedom manipulator," *SICE*, vol. 22, no. 3, pp. 343–350, 1986 (in Japanese).
5. R. P. Paul and B. Shimano, "Compliance and control," *Proc. JACC*, pp. 694–699, 1976.
6. D. E. Whitney, "Force feedback control of manipulator fine motions," *ASME J. Dyn. Syst. Meas. Control*, vol. 98, pp. 91–97, 1977.
7. N. Hogan, "Impedance control: an approach to manipulation. Part I—Theory. Part II—Implementation. Part III—Applications," *J. Dyn. Syst. Meas. Control*, vol. 101, pp. 1–24, 1985.
8. N. Hogan, "Stable execution of contact tasks using impedance control," *Proc. IEEE Conf. Robotics Automation*, pp. 1047–1054, 1987.
9. C. H. An and J. M. Hollerbach, "Dynamic stability issues in force control of manipulators," *Proc. IEEE Conf. Robotics Automation*, pp. 890–896, 1987.
10. H. Inoue, "Computer control of an artificial hand," *J. Jpn Soc. Mech. Eng.*, vol. 73, no. 718, pp. 946–954, 1970 (in Japanese).
11. S. Kurono, "Study of motion control of a pair of artificial hands," *J. Jpn Soc. Mech. Eng.*, vol. 78, no. 682, pp. 804–810, 1975 (in Japanese).
12. M. Uchiyama, "Study on dynamic control of an artificial hand (coordination motion control with a mathematical model)," *Trans. Jpn Soc. Mech. Eng.*, vol. 45, no. 391, pp. 323–335, 1979.
13. H. Arai and S. Tachi, "Force detection and active power assistance of a direct-drive manipulator," *Adv. Robotics*, vol. 2, no. 3, pp. 241–257, 1987.
14. R. P. Paul, *Robot Manipulators: Mathematics, Programming, and Control.* Cambridge, MA: MIT Press, 1981.
15. J. J. Craig, *Introduction to Robotics Mechanics and Control.* Addison-Wesley, 1986.
16. H. Asada, *Direct-Drive Robots: Theory and Practice.* Cambridge, MA: MIT Press, 1987.
17. T. Suehiro and K. Takase, "Manipulation system based on task coordinate servo mechanism by direct computational method," *J. Robotics Soc. Jpn*, vol. 3, no. 2, pp. 95–105, 1985 (in Japanese).
18. H. Arai and S. Tachi, "Development of a power-assisted head-coupled display system for tele-existence," *Mech. Eng. Lab. Rep.*, vol. 42, no. 5, 1988 (in Japanese).
19. S. Komada, T. Murakami, T. Hoshinaka and K. Onishi, "Force feedback control of a multi-dimensional robot," *Nat. Rec. IEE Jpn*, pp. 707–712, 1987 (in Japanese).

APPENDIX: 1. EQUATION OF MOTION FOR THE TWO-DEGREE-OF-FREEDOM MANIPULATOR

The Lagrange equation of motion was applied to the 2 DOF manipulator shown in Fig. A1.

Kinetic energy:

$$\begin{aligned} I = {} & (1/2)J_{g2}\dot{\theta}_2^2 + (M_2/2)[\{\mathrm{d}(l_2 \sin\theta_2)/\mathrm{d}t\}^2 + \{\mathrm{d}(-l_2\cos\theta_2)/\mathrm{d}t\}^2] \\ & + (1/2)J_{g3}\dot{\theta}_3^2 + (M_3/2)[\{\mathrm{d}(L_2\sin\theta_2 + l_3\sin\theta_3)/\mathrm{d}t\}^2 \\ & + \{\mathrm{d}(L_2\cos\theta_2 + l_3\cos\theta_3)/\mathrm{d}t\}^2]. \end{aligned} \tag{A1}$$

Potential energy:

$$\begin{aligned} U = {} & M_2 g l_2(1-\cos\theta_2) \\ & + M_3 g[(L_2 + l_3) - (L_2\cos\theta_2 + l_3\cos\theta_3)]. \end{aligned} \tag{A2}$$

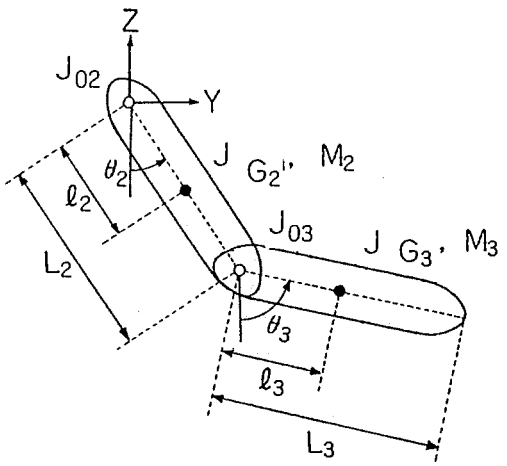

M_i : mass of link i

J_{0i} : moment of inertia of link i about joint i

J_{Gi} : moment of inertia of link i about the center of gravity of link i

ℓ_i : length between joint i and the center of gravety of link i

L_i : length of link i

Figure A1. Dynamic model of a two d.o.f. manipulator.

Dissipation energy:

$$D = (1/2)D_2\dot{\theta}_2^2 + (1/2)D_3(\dot{\theta}_3 - \dot{\theta}_2)^2. \tag{A3}$$

Lagrange equation of motion:

$$\mathrm{d}(\partial I/\partial\dot{\theta}_i)/\mathrm{d}t - \partial I/\partial\theta_i + \partial U/\partial\theta_i + \partial D/\partial\dot{\theta}_i = T_{a,i} \quad (i = 2, 3). \tag{A4}$$

The manipulator's equation of motion is as follows:

$$\begin{bmatrix} J_{02} + M_3L_2^2 & M_3L_2l_3\cos(\theta_2 - \theta_3) \\ M_3L_2l_3\cos(\theta_2 - \theta_3) & J_{03} \end{bmatrix}\begin{bmatrix}\ddot{\theta}_2 \\ \ddot{\theta}_3\end{bmatrix} + \begin{bmatrix} D_2 + D_3 & -D_3 \\ -D_3 & D_3 \end{bmatrix}\begin{bmatrix}\dot{\theta}_2 \\ \dot{\theta}_3\end{bmatrix} = \begin{bmatrix} T_{a,2} - T_{a,3} - T_{c,1} \\ T_{a,3} - T_{c,2} \end{bmatrix} \tag{A5}$$

where

$$T_{c,1} = M_3L_2l_3\sin(\theta_2 - \theta_3)\dot{\theta}_3^2 + (M_2l_2 + M_3L_2)g\sin\theta_2 \tag{A6}$$

$$T_{c,2} = -M_3L_2l_3\sin(\theta_2 - \theta_3)\dot{\theta}_2^2 + M_3l_3g\sin\theta_3. \tag{A7}$$

This is employed as follows:

$$I\ddot{\Theta} + D\dot{\Theta} = T_a - T_c \tag{A8}$$

where

$$T_a = \begin{bmatrix} T_{a,2} \\ T_{a,3} \end{bmatrix}, \quad T_c = \begin{bmatrix} T_{a,3} + T_{c,1} \\ T_{c,2} \end{bmatrix}.$$

APPENDIX 2: IDENTIFICATION OF THE DYNAMICS OF A RIGID PENDULUM

As we discussed in Section 3.3, the equation of motion of a rigid pendulum is

$$I\ddot{\theta} + D_v\dot{\theta} + C_r = -K\theta. \tag{A9}$$

By measuring the amplitude and period of the step response with spring coefficient K, the damping ratio ζ, the natural frequency f_r and the Coulomb friction coefficient C_r are calculated. This calculation uses the following equations:

$$X_k = X_{k+1} \exp[\pi\zeta/\sqrt{1-\zeta^2}] + 2A(1 + \exp]\pi\zeta/\sqrt{1-\zeta^2}]), \tag{A10}$$

where X_k, X_{k+1} $(k = 1, 2, \ldots)$ is the double amplitude and A is the spring deflection caused by the Coulomb friction.

The following relationships are used when calculating the desired parameters I, D_v, and C_r.

$$\zeta = D_v/(2\sqrt{KI}) \quad \text{damping ratio} \tag{A11a}$$

$$f_r = (1/2\pi)(\sqrt{K/I}) \quad \text{natural frequency} \tag{A11b}$$

$$A = C_r/K \tag{A11c}$$

APPENDIX 3: ASSIGNMENT OF THE TARGET IMPEDANCE

The equation of motion for a system having the desired target impedance is given as follows:

$$F_e = M\ddot{\theta} + B\dot{\theta} + K(\theta - \theta_0). \tag{A12}$$

The following two methods are used when assigning the target impedance:

(1) Direct assignment of M, B, K.
(2) Assigning the natural frequency f_r, the damping ratio ζ, and the inertia ratio ϕ for the apparent inertia as opposed to the actual intertia.

That is,

$$M = I(\phi/100) \tag{A13a}$$

$$K = (2\pi f_r)^2 M \tag{A13b}$$

$$B = 2\zeta\sqrt{KM}. \tag{A13c}$$

If coefficients M, B, and K—derived from either (1) or (2)—are substituted into the following equation, we can derive the required actuator output torque needed to obtain the target impedance for the system shown in (A9).

$$T_a = (I - M)\ddot{\theta} + (D_v - B)\dot{\theta} + K(\theta_0 - \theta) + C(\theta, \dot{\theta}). \tag{A14}$$

APPENDIX 4: DRIVE TORQUE DURING IMPEDANCE CONTROL

The following equation is the manipulator's equation of motion when the external force F_e is applied:

$$I\ddot{\Theta} + D\dot{\Theta} = T_a - T_c + J^T F_e. \tag{A15}$$

The equation of motion for the system having the desired target impedance of equation (2) opposed to external force F_e is

$$F_e = M\ddot{X} + B\dot{X} + K(X - X_0). \tag{A16}$$

If the actuator output torque is established in the following way, control can be performed according to the impedance given in equation (2).

$$T_a = (I - J^T MJ)\ddot{\Theta} + (D - J^T M\dot{J} - J^T BJ)\dot{\Theta} + J^T K(X_0 - L(\Theta)) + T_c. \tag{A17}$$

The desired target impedance parameters were set as follows:

$$M = \begin{bmatrix} m_y & 0 \\ 0 & m_z \end{bmatrix}, \quad B = \begin{bmatrix} b_y & 0 \\ 0 & b_z \end{bmatrix}, \quad K = \begin{bmatrix} k_y & 0 \\ 0 & k_z \end{bmatrix}, \quad x_0 = \begin{bmatrix} y_0 \\ z_0 \end{bmatrix}. \tag{A18}$$

The outputs for each of the actuators of the manipulator in Appendix 1 are calculated as follows:

$$\begin{aligned} T_{a,2} = {} & [J_{02} + M_3 L_2^2 - L_2^2(C_2^2 m_y + S_2^2 M_z)]\ddot{\theta}_2 \\ & + [M_3 l_3 L_2 C_{23} - L_2 L_3(C_2 C_3 m_y + S_2 S_3 m_z)]\ddot{\theta}_3 \\ & + [D_2 + D_3 - L_2^2(C_2^2 b_y + S_2^2 b_z)]\dot{\theta}_2 \\ & + [-D_3 - L_2 L_3(C_2 C_3 b_y + S_2 S_3 b_z)]\dot{\theta}_3 \\ & + [L_2 C_2 k_y(y_0 - L_2 S_2 - L_3 S_3) + L_2 S_2 k_z(z_0 + L_2 C_2 + L_3 C_3)] \\ & - T_{a,3} + T'_{c,1} \end{aligned} \tag{A19}$$

$$\begin{aligned} T_{a,3} = {} & [M_3 l_3 L_2 C_{23} - L_2 L_3(C_2 C_3 m_y + S_2 S_3 m_z)]\ddot{\theta}_2 \\ & + [J_{03} - L_3^2(C_3^2 m_y + S_3^2 m_z)]\ddot{\theta}_3 \\ & + [-D_3 - L_2 L_3(C_2 C_3 b_y + S_2 S_3 b_z)]\dot{\theta}_2 \\ & + [D_3 - L_3^2(C_3^2 b_y + S_3^2 b_z)]\dot{\theta}_3 \\ & + [L_3 C_3 k_y(y_0 - L_2 S_2 - L_3 S_3) + L_3 S_3 k_z(z_0 + L_2 C_2 + L_3 C_3)] \\ & + T'_{c,2} \end{aligned} \tag{A20}$$

where

$$\begin{aligned} C_i &= \cos\theta_i, \quad i = 2, 3 \\ S_i &= \sin\theta_i, \quad i = 2, 3 \\ C_{23} &= \cos(\theta_2 - \theta_3) \\ S_{23} &= \sin(\theta_2 - \theta_3) \end{aligned}$$

$$T'_{c,1} = T_{c,1} + L_2^2 C_2 S_2(m_y - m_z)\dot{\theta}_2^2 + L_2 L_3(C_2 S_3 m_y - S_2 C_3 m_z)\dot{\theta}_3^2 \tag{A21}$$

$$T'_{c,2} = T_{c,2} + L_3^2 C_3 S_3(m_y - m_z)\dot{\theta}_3^2 + L_2 L_3(S_2 C_3 m_y - C_2 S_3 m_z)\dot{\theta}_2^2. \tag{A22}$$

APPENDIX 5: IMPEDANCE CONTROLLABLE SPACE

In experiment (2) of Section 4.2, because the actual inertia changes due to the end-effector's position, a large discrepancy can be created between the actual inertia and

the virtual inertia. This can cause the actuator to exceed its output limits. It can even cause oscillations which make it impossible for the manipulator to be controlled according to the target impedance. Therefore, it is important to consider the limits of possible target impedance for the manipulator.

Generally, for an m degree-of-freedom manipulator operating in an n-dimensional space R, the following vector space is defined:

$$P = \begin{bmatrix} p_1 \\ \vdots \\ p_m \end{bmatrix}, \; p_1, \ldots, p_m\text{: output for each actuator}$$

and according to Appendix 2,

$$\phi = \begin{bmatrix} \phi_1 \\ \vdots \\ \phi_n \end{bmatrix}, \qquad F_r = \begin{bmatrix} f_{r,1} \\ \vdots \\ f_{r,n} \end{bmatrix}, \qquad \zeta = \begin{bmatrix} \zeta_1 \\ \vdots \\ \zeta_n \end{bmatrix}.$$

This being the case,

$$p_1 < q_1, \ldots, p_m < q_m$$
$$q_1, \ldots, q_m : \text{output limit for each actuator.}$$

From equation (15) and this condition, θ, F_r, and ζ are given certain restrictions. Because the actual inertia is decided for the points in space R of the working space, we can decide the impedance control possibilities for space Ω including vector spaces P, θ, F_r, ζ, and R:

$$\Omega = \Omega(P, \phi, F_r, \zeta, R).$$

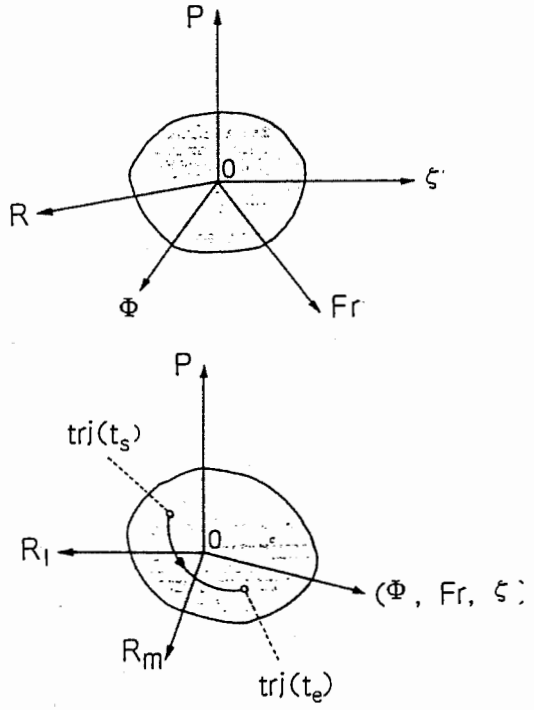

Figure A2. Impedance controllable space.

We will call this the impedance controllable space. The impedance controllable space Ω is shown conceptually in Fig. A2.

This is applied, for example, in the following way:

(1) The impedance controllable space Ω is determined based on the working space R and the performance of the manipulator's actuators. When the manipulator operates along a particular trajectory of space R of the working space, a check is made to determined whether the established target impedance $(\phi(t), F_r(t), \zeta(t))$ are included in space Ω for each point trj(t) within that trajectory. If some points are not included in space Ω, either the trajectory or the target impedance is modified.

(2) When we want to perform operations following a trajectory between the two points trj(t_s) and trj(t_e) in space R of the working space, if $\int_{t_s}^{t_e} |P(t)| \, dt$ for the target impedance is minimized, the most energy-efficient trajectory can be established.

ABOUT THE AUTHORS

Susumu Tachi (M'83) was born in Tokyo on 1 January 1946. He received B.E., M.S., and Ph.D. degrees in mathematical engineering and information physics from the University of Tokyo in 1968, 1970, and 1973, respectively. He joined the Faculty of Engineering, University of Tokyo, in 1973. In 1975, he joined the Mechanical Engineering Laboratory, Ministry of International Trade and Industry, Tsukuba Science City, where he served as Director of the Biorobotics Division. From 1979 to 1980, he was a Japanese Government Award Senior Visiting Fellow at the Massachusetts Institute of Technology, Cambridge, MA, U.S.A. Dr. Tachi is currently Associate Professor of the University of Tokyo. His present interests include human rehabilitation engineering, statistical signal analysis, and robotics—in particular, sensory control of robots, autonomous mobile robots, and tele-robotics. Dr Tachi is a founding director of the Robotics Society of Japan, and a fellow of the Society of Instrument and Control Engineers.

Taisuke Sakaki (M'87) was born in Fukuoka, Japan on 5 November 1960. He received a B.S. degree from Kyusyu University in 1984. From 1984 he worked at Yaskawa Electric Company. From 1986 to 1988 he was a guest researcher at the Mechanical Engineering Laboratory, Tsukuba Science City, Japan. His interests include manipulator control and master–slave systems. He is a member of the Society of Instrument and Control Engineers, and the Robotics Society of Japan.

Hirohiko Arai (M'83) was born in Tokyo on 9 July 1959. He graduated from the University of Tokyo in 1982, majoring in instrument engineering. In 1982, he joined Honda Engineering Corporation. In 1984, he joined the Mechanical Engineering Laboratory, Ministry of International Trade and Industry, Tsukuba Science City, and is currently a researcher for the Biorobotics Division of the Robotics Department. His interests include manipulator control, man–machine systems, and tele-operation. He is a member of the Society of Instrument and Control Engineers, the Japan Society of Mechanical Engineers, and the Robotics Society of Japan.

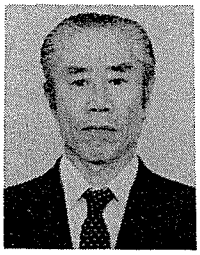

Shoichiro Nishizawa was born on 28 December 1928 in Tokyo, Japan. He joined the Mechanical Engineering Laboratory, Ministry of International Trade and Industry in 1945. He was a Senior Researcher of the Biorobotics Division of the Robotics Department. He retired in 1989.

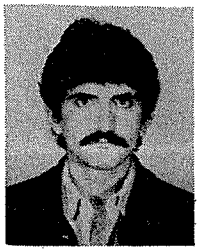

Jose Felipe Pelaez Polo was born in Cuernavaca, Morelos, Mexico on 28 April 1961. He graduated from Universidad Autonoma Metropolitana in 1984, majoring in mechanical engineering. He worked for Nissan Mexicana from 1984 to 1986, and was a visiting researcher at the Mechanical Engineering Laboratory, Ministery of International Trade and Industry, Japan, from 1986 to 1987. He is currently an assistant professor of the Universidad Nacional Autonoma de Mexico (UNAM).